**Showcasing research from Professor Dehnen's laboratory, Institute of Nanotechnology, Karlsruhe Institute of Technology, Germany.**

From non-innocent ionic liquids to reactive agents in the synthesis of chalcogenido metalate compounds

The work highlights the non-innocent character of imidazolium-based ionic liquids in the synthesis of chalcogenido metalates, which are affected in a variety of ways, including the derivatization of the anionic substructures with corresponding consequences on the properties of the products.

Image reproduced by permission of Stefanie Dehnen from *Chem. Commun.*, 2025, **61**, 17530.

As featured in:
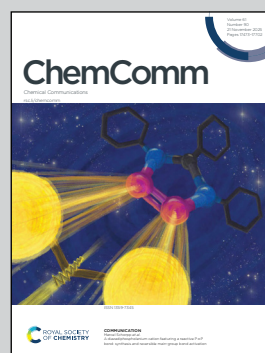
See Stefanie Dehnen *et al.*,
Chem. Commun., 2025, **61**, 17530.

ROYAL SOCIETY OF CHEMISTRY

rsc.li/chemcomm

Check for updates

From non-innocent ionic liquids to reactive agents in the synthesis of chalcogenido metalate compounds

Gina Stuhrmann, [iD] Bastian Weinert [iD] and Stefanie Dehnen [iD] *

Chalcogenido metalate compounds are an exceptional class of inorganic materials, ranging from discrete clusters and simple binary solids to complex multinary three-dimensional structures with open frameworks. This structural and compositional diversity generally enables a wide range of applications, including opto-electronics, ion separation and catalysis. Traditionally, chalcogenido metalates have been synthesized using flux synthesis or high-temperature solid-state reactions as well as solvothermal approaches. More recently, this was shifted towards lower-temperature approaches, not only for economic and environmental reasons, but also to access previously inaccessible compounds. In this context, ionic liquids (ILs) have become important reaction media. However, while ILs have been famous for their role as inert reaction media that provide a controlled environment for crystallization, they can also be actively involved in the reactions under certain conditions and thus influence the formation and stabilization of the new chalcogenido metalate compounds. This can take place by adopting a templating role or through the transfer of (functional) groups, which enables access to modifications and variations of the corresponding substructures. This dual role of ILs—as reaction media and reactive agents—provides new opportunities for fine-tuning the structural and electronic properties of chalcogenido metalate compounds. In this review, the multifaceted roles of non-innocent ILs in the synthesis of chalcogenido metalate compounds are explored, with particular attention on their effects on cluster formation, cluster stability, and their ultimate effect on the compounds' properties.

Institute of Nanotechnology, Karlsruhe Institute of Technology, Kaiserstrasse 12, 76131 Karlsruhe, Germany. E-mail: stefanie.dehnen@kit.edu

Dr Gina Stuhrmann studied chemistry, German language, and literature, as well as education at Philipps University Marburg and graduated in 2021. She completed her PhD in inorganic chemistry under supervision of Stefanie Dehnen at the Karlsruhe Institute of Technology in 2024, focusing on the synthesis and characterization of chalcogenido metalate compounds from ionothermal reactions. During her doctoral studies, she was awarded a DAAD scholarship, which enabled her to conduct a research stay in the group of Mercouri Kanatzidis at Northwestern University (IL, USA), expanding her expertise in solid-state chemistry. Currently, she is a postdoctoral research fellow in the Dehnen group, where her research focuses on the reactivity of chalcogenidotitanates in ionic liquids.

Gina Stuhrmann

Dr Bastian Weinert studied chemistry at the Philipps University Marburg and graduated in 2011. He completed his PhD in inorganic chemistry under supervision of Stefanie Dehnen in 2014, focusing on the synthesis and characterization of compounds with multinary intermetalloid clusters and Zintl anions. During his doctoral studies, he was awarded a scholarship from Fonds der Chemischen Industry (FCI). Currently, he is group leader and Akademischer Rat in the Dehnen group at Institute of Nanotechnology, Karlsruhe Institute of Technology, where his research focuses on compounds with multinary and non-classical chalcogenido metalates.

Bastian Weinert

Introduction

Chalcogenido metalate compounds, with anionic substructures ranging from isolated clusters to three-dimensional frameworks, have long been a focus of inorganic and materials chemistry. This is due to their unique structural and chemical properties, which make them perfect candidates for potential applications, such as gas and ion storage materials, ionic conductors, or materials for (photo)catalytic H_2 evolution, to mention but a few.[1–7] In addition, many chalcogenido metalates are characterized by interesting physical (especially, opto-electronic) properties. These include intense photoluminescence, high photoconductivity, or frequency doubling.[8–13] Of particular interest are porous chalcogenido metalates, which exhibit tuneable pore sizes and are promising as selective ion exchange materials.[14–17] The incorporation of different metal ions, such as p- and d-block elements, into such structures significantly enhances their diversity and allows for fine-tuning of their physicochemical properties.[18–20] Compounds with pure p-block chalcogenido metalate substructures, such as the 3D-$[Sn_2S_5]^{2-}$ framework, have been used as robust and cost-effective materials for the recovery of rare earth elements.[21]

The development of crystalline chalcogenido metalate compounds with novel compositions and architectures has become a key area of materials research today, for which the development of innovative synthesis methods is essential.[22,23] The synthesis of chalcogenido metalate compounds is typically categorized according to the temperature range of the reactions. High-temperature methods include classical solid-state
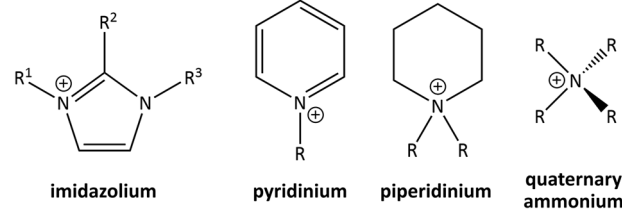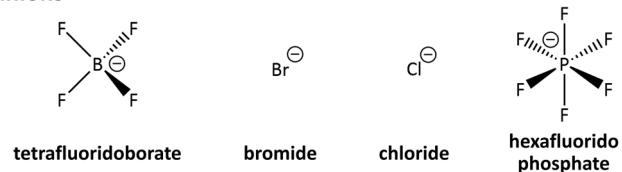

Fig. 1 Summary of common cations and anions combined in ionic liquids for ionothermal reactions (R: alkyl groups).

reactions and molten flux techniques, while low-temperature approaches include wet-chemical and solvothermal processes.[24–27] Solid-state reactions carried out at temperatures above 600 °C are diffusion-controlled and favour the generation of thermodynamically stable compounds. The limited kinetic control results in difficulties to influence products design.[28–31] In contrast, molten flux techniques are carried out at comparatively lower temperatures (200–600 °C), determined by the melting point of the excess alkali/alkaline earth chalcogenide used as flux.[32–34] Flux reactions also include metallic fluxes, such as the reaction of K_2Te and $HgTe$ in liquid mercury yielding $K_2[Hg_2Te_3]$ with a 3D-network structure composed of corner-linked $\{HgTe_4\}$ tetrahedra.[35] Wet-chemical syntheses temperatures are limited by the boiling temperature of the solvent used. While high temperatures favour extended 2D- or 3D-networks, wet-chemical methods thus typically lead to compounds with discrete anionic clusters (0D) or 1D structures.[36–38] Solvothermal reactions, which take place under supercritical conditions, involve elevated temperatures and pressures depending on the vapour pressure of the solvent used. Although these conditions pose safety risks, they allow the synthesis of unique structures by offering a wide range of solvents.[39] In addition, solvothermal methods facilitate the formation of inorganic–organic hybrid compounds containing amines, in situ derived ammonium counterions, or transition-metal complexes also generated in situ by combining donor solvent molecules with metal ions from the reaction mixture.[40–44]

The search for novel structures and properties of chalcogenido metalate compounds has driven the development of innovative synthetic strategies. More recent achievements include unconventional reaction conditions with the usage of ionothermal, surfactant-thermal and hydrazine-thermal methods.[45–50] Among these, ionothermal syntheses are characterized by the fact that they operate at low temperatures (<200 °C), using ionic liquids (ILs) as reaction media without the addition of conventional solvents. ILs are salts with low melting temperatures (m.t. < 100 °C) due to the poor interaction between their anions and cations, resulting in low lattice energies.[51–53]

Stefanie Dehnen is a Professor of Information-Based Materials Design and Nanosciences as well as of Inorganic Chemistry at Karlsruhe Institute of Technology (KIT) and Executive Director of the Institute of Nanotechnology (INT) at KIT. She is a member of seven national and international scientific academies, including Leopoldina–German National Academy of Sciences, European Academy of Sciences (EurASc) and the Academia Europaea–Academy of Europe, and

Stefanie Dehnen

she has been awarded many prestigious prizes and grants during her career, including the Gottfried Wilhelm Leibniz Prize from the German Research Foundation (DFG)—the most prestigious German-based research award—and an ERC Advanced Grant by the European Research Council. Currently, Stefanie Dehnen is the Editor-in-Chief of the journal Inorganic Chemistry (American Chemical Society, ACS) and the President of the German Chemical Society (GDCh). She is an expert for cluster-based materials, focusing on compounds with multinary, in particular multimetallic, molecular nanoarchitectures that exhibit potential as innovative catalysts, white-light emitters or battery materials.

Although Walden reported such a low-melting salt, ethylammonium nitrate (m.t. 12 °C) as early as in 1914, the term "ionic liquid" was introduced much later.[54,55]

As shown in Fig. 1, typical ILs consist of organic cations (e.g., imidazolium, pyridinium, piperidinium, or quaternary ammonium) and simple or weakly interacting anions (e.g., halides, $[BF_4]^-$, or $[PF_6]^-$).[22] ILs offer several advantages over other classical solvents, including lower vapour and reaction pressures, improved thermal stability, and excellent solvation properties. Ionic liquids also contribute to the concept of green chemistry by minimizing waste generation and enabling more efficient recycling.[56–60] In addition, ILs can be used as "designer solvents" due to the large number of different and customizable cation–anion combinations.[61] These properties and the diversity make them highly suitable for the efficient and sustainable synthesis of novel crystalline materials via ionothermal reactions. Today, ILs are widely applied in ionothermal synthesis, hence, at elevated temperatures in sealed ampoules and well below supercritical conditions. This approach has meanwhile served to generate numerous crystalline materials, including zeolites, organometallic frameworks and chalcogenido metalates.[62,63]

Although ILs are widely regarded as inert reaction media, in some cases, they also actively participate in reactions, thus exhibiting a non-innocent behaviour. The active participation of non-innocent ILs has been reported for various research areas,[64–69] which was recently reviewed comprehensively by Ruck and co-workers.[62]

The ILs' multifunctionality is also evident in the field of CO_2 capture and conversion, where ILs influence separation, activation, and catalytic transformation pathways.[70] A similar phenomenon is observed in lithium-ion batteries, where exothermic reactions with electrodes highlight the active role of ILs beyond that of inert electrolytes.[71]

Their tunable structures and versatility make ILs particularly valuable for emerging energy technologies, such as thermal energy storage, nitrogen reduction for ammonia production, and aluminium-ion batteries, where they can be precisely adapted to the requirements of each application.[72]

ILs containing reactive moieties, can directly contribute to the composition of the final products. For instance, ILs with halide-based anions have been shown to act as both solvents and halogen source in the synthesis of complex borate halide compounds and other crystalline frameworks.[73–76] These findings enable innovative synthetic strategies for different types of inorganic materials.[77,78]

This feature article focuses on the dual functionality of non-innocent ILs in the context of ionothermal syntheses of chalcogenido metalate compounds.[79–81] We aim to provide a detailed and comprehensive overview of the unique contributions of ILs to this specific field, with a particular focus on their role in enabling the discovery and formation of new structures. However, it should be noted that ILs do not necessarily have a strictly defined non-innocent behaviour, as their interactions within a reaction system can be dynamic and overlapping.[82,83]

Influence of ILs cations on structure assembly

Literature reports on the synthesis of chalcogenido metalates from ILs predominantly describe the use of imidazolium-based ILs, which are systematically abbreviated as follows. They are denoted as $(C_l(C_m)C_nIm)^+$, where l, m and n represent the number of carbon atoms in the (linear) alkyl chains attached to the N1-, C2-, and N3-position of the imidazolium (Im) ring, respectively. Neutral imidazoles are denoted as "im" for discrimination.[84,85] Of particular importance of the non-innocent behaviour of ILs is the incorporation of their cations (or anions) into the final products, often acting as counterions to balance the charge of ionic substructures of the opposite charge. These can be encapsulated or separated by the organic cations of the ILs. Anion···π or anion···H interactions between chalcogenide ligands and organic IL cations contribute to the enhanced stability of the resulting compounds. This interaction is rarely observed in traditional low temperature methods.[86,87]

In order to emphasize the role of ILs as non-innocent components in the synthesis of crystalline chalcogenido metalates, systematic experiments were conducted using different starting materials, with or without $SnCl_4 \cdot 5H_2O$ in various ILs. This approach yielded novel chalcogenido metalate compounds with diverse dimensionalities of the anionic part, including 1D-strands in $(C_4C_1C_1Im)_2[Ge_4SnSe_{10}]$, 2D-layers in $(C_4C_1C_1Im)_2[Ge_{0.83}Sn_{3.17}Se_{9.06}]$, and extended 3D-open frameworks such as in $(C_4C_1Im)_4[Sn_9Se_{20}]$ and $(C_4C_1C_1Im)_8[Sn_{18}Se_{40}]$.

The anions are illustrated in Fig. 2. The 1D-$[Ge_4SnSe_{10}]^{2-}$ anion is composed of $\{Ge_4Se_{10}\}$ units linked by three-coordinated Sn^{II} atoms to form infinite double chains. The 2D-$[Ge_{0.83}Sn_{3.17}Se_{9.06}]^{2-}$ anion consists of one $\{Sn_6Se_{10}\}$ unit and two $\{Ge_{0.83}Sn_{0.17}Se_{4.06}\}$ tetrahedra with mixed Ge/Sn positions that are connected to form 2D-layers. The structure of $[Sn_9Se_{20}]^{4-}$ features $\{Sn_3Se_4\}$ defect-heterocubanes connected by two μ-Se bridges, forming $\{Sn_2S_2\}$ rings. These units are further linked through $\{SnSe_4\}$ tetrahedra into the 3D network. In $(C_4C_1C_1Im)_8[Sn_{18}Se_{40}]$, the anionic 3D structure is made up of $\{Sn_3Se_4\}$ defect-heterocubanes, connected by $\{Sn_3Se_{10}\}$ subunits. The dimensional variations, along with different elemental compositions, affect the photo-optical properties of the crystalline solids. The incorporation of Sn^{II} atoms as linkers between the $\{Ge_4Se_{10}\}$ units results in a slight red shift for 1D-$(C_4C_1C_1Im)_2[Ge_4SnSe_{10}]$, to 2.33 eV, while in 2D-$(C_4C_1C_1Im)_2[Ge_{0.83}Sn_{3.17}Se_{9.06}]$, the larger Sn/Se building units causes a more pronounced red shift, along with a second absorption onset at 2.25 eV, reflecting the additional contribution of the Ge/Se units to the optical features. The network compound 3D-$(C_4C_1Im)_4[Sn_9Se_{20}]$, which contains no Ge, exhibits a bandgap of 2.2–2.3 eV.[88–90] It is noteworthy that certain selenido metalates could also be synthesized directly from elemental tin and selenium in $(C_4C_1C_1Im)Cl$, thereby highlighting the versatility and non-innocent role of ILs in these formation procedures.[91] All of the structures possess voids that are filled with the IL cations, which emphasizes the influence of these species:
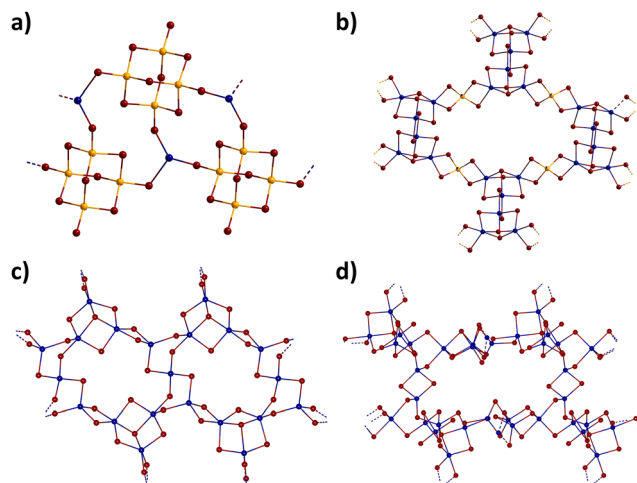
Fig. 2 Depiction of (a) $(C_4C_1C_1Im)_2[Ge_4SnSe_{10}]$, (b) $(C_4C_1Im)_4[Sn_9Se_{20}]$, (c) $(C_4C_1C_1Im)_2[Ge_{0.83}Sn_{3.17}Se_{9.06}]$, and (d) $(C_4C_1Im)_2[Sn_{18}Se_{40}]$. Colour code: Sn = dark blue, Ge = light orange, Se = dark red.

Fig. 3 Structure of the anions in (a) $(C_2C_1Im)_4[Ge_4Se_{10}]$, (b) $(C_2C_1Im)_6$-$[Ge_8Se_{19}]$ and (c) $(C_2C_1Im)_8[Ge_{16}Se_{36}]$. (d) Schematic representation of the strategy for reducing the average charge of supertetrahedral chalcogenide cluster anions through the formation of discrete cluster oligomers. Panel (d) adopted with permission from ACS. Colour code: Ge = light orange, Se = dark red.

definitely through assistance with the crystallization of specific species, but possibly also through assistance at the assembly of the mentioned structural moieties.

Building upon this concept, the use of ILs with a non-innocent behaviour has also proven fruitful in the assembly of finite cluster oligomers, thereby enhancing solubility without affecting opto-electronic properties in an unwanted way. Treatment of $Na_4[GeSe_4]\cdot14H_2O$ or $K_4[Ge_4Se_{10}]\cdot3H_2O$ in $(C_2C_1Im)^+$-based ILs yielded condensation products of the T2-type $[Ge_4Se_{10}]^{4-}$ anion (Fig. 3(a)). Dimeric $[Ge_8Se_{19}]^{6-}$ (Fig. 3(b)) and tetrameric $[Ge_{16}Se_{36}]^{8-}$ (Fig. 3(c)) structures were isolated as single-crystalline salts. According to the literature, the relative amount of the auxiliary DMMP is proposed to mediate the release of Se^{2-} anions, most likely as H_2Se, through deprotonation of H_2O and subsequent hydrogen bonding with the selenido germanate units. Different DMMP-to-IL ratios were suggested to influence the degree of cluster aggregation and local tetramerization, although no *in situ* mechanistic studies have been conducted. The charge per cluster unit decreases gradually from 4− in the parent cluster to 3− in the dimer and 2− in the tetramer (Fig. 3(d)). The reduction in charge per cluster unit results in a weakening of the electrostatic interactions between anions and cations, thereby facilitating the dissolution of the salts in DMF (DMF = dimethylformamide). ESI mass spectrometry (ESI = electrospray ionization) and dynamic light scattering studies further demonstrated the change in cation···anion interactions. Optical absorption measurements confirmed a consistent decrease in optical gaps as the cluster size increased, with the same trend being observed both in solution and in the solid state.[92]

Four single-crystalline nickel chalcogenido phosphates were synthesized ionothermally in $(C_2C_1Im)BF_4$ at 150 °C, yielding salts of $[Ni(P_2S_8)_2]^{2-}$, $[Ni(P_3S_9)(P_2S_8)]^{3-}$, $[Ni(P_3S_9)_2]^{4-}$, and $[(NiP_3S_8)_4(PS_4)]^{7-}$. The molecular anionic structures of the first three compounds show a single Ni atom in octahedral coordination by six S atoms, whereas $[(NiP_3S_8)_4(PS_4)]^{7-}$ contains four Ni atoms, each coordinated by five S atoms and one P atom. In all of these
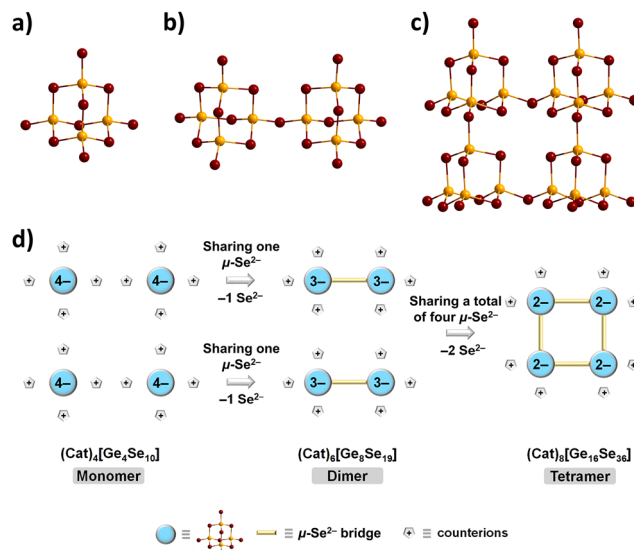
compounds, the P atoms are surrounded by four S atoms in a tetrahedral fashion, forming distinct $[P_xS_y]^{n-}$ ligands. Although these binary P–S ligands had been previously known, their coordination modes were novel in that report. The anion $[Ni(P_2S_8)_2]^{2-}$ consists of two {PS_4} units sharing a S corner atom, with two additional corners bridged by a trisulfide group (Fig. 4(a)). In $[Ni(P_3S_9)(P_2S_8)]^{3-}$, the Ni atom interacts with two different ligands: a $[P_2S_8]^{2-}$ ligand, which coordinates similarly to that in $[Ni(P_2S_8)_2]^{2-}$, and a $[P_3S_9]^{3-}$ ligand, which is composed of three corner-sharing {PS_4} units (Fig. 4(b)). By expanding on the coordination motifs observed earlier, $[Ni(P_3S_9)_2]^{4-}$ incorporates a Ni centre bound to two $[P_3S_9]^{3-}$ ligands (Fig. 4(c)). The complex anionic structure of $[(NiP_3S_8)_4(PS_4)]^{7-}$ consists of a central {PS_4} unit surrounded by four interconnected {NiP_3S_8} groups. Each Ni atom is coordinated by two S atoms and one P atom from a {P_3S_8} moiety, together with a S atom from an adjacent {P_3S_8} ligand (Fig. 4(d)). Notably, in the thiophosphate ligand the S as well as the P atoms act as donors, which results in an unprecedented coordination mode.[47] The cations of the ILs used in these syntheses act as counterions, and as such, represent an important

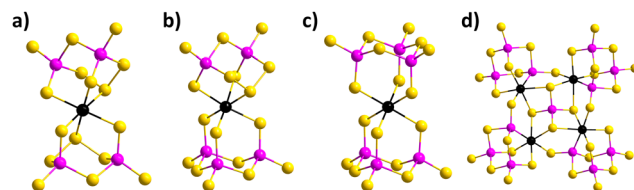Fig. 4 Molecular structures of the nickel thiophosphate anions of (a) $(C_2C_1Im)_2[Ni(P_2S_8)_2]$, (b) $(C_2C_1Im)_3[Ni(P_3S_9)(P_2S_8)]$, (c) $(C_2C_1Im)_4[Ni(P_3S_9)_2]$, and (d) $(C_2C_1Im)_7[(NiP_3S_8)_4(PS_4)]$. Colour code: Ni = black, P = pink, S = gold.

part of the reaction products itself. This behaviour highlights the role of ILs also as a structure-directing agent (SDA) without influencing the architecture of the moieties that are surrounded by the IL components themselves.[86,87,93] Such distinct effects and interactions are rarely observed in conventional low-temperature solvent methods.[94] The SDA behaviour was first developed in 2004 for the synthesis of zeolites using eutectic mixtures of $(C_2C_1Im)Br$ and urea/choline chloride.[95] In contrast to traditional hydrothermal techniques, the simultaneous use of the IL (cations) as reaction medium and template prevents competition between solvent and template during product formation, thereby enhancing structural development. This advantage is particularly important for the controlled synthesis of porous crystalline materials.[25] Furthermore, anion$\cdots\pi$ interactions between the chalcogenide ions and the organic cations contribute to the increased stability of discrete clusters, strengthening the frameworks and facilitating the formation of novel and often unprecedented cluster structures.

There are many more examples for this role, but we decided to focus on a brief overview here as we aim to explore additional aspects of the non-innocent behaviour of ILs in this feature article.

One more parameter to be named here in addition to the general role of the ionic liquids is the absence or presence of an auxiliary. The synthesis of crystalline open-framework selenido stannates was explored employing imidazolium-based ILs with (again) varying alkyl chain lengths, thereby introducing $N_2H_4\cdot H_2O$ as a co-solvent. This enabled the synthesis of compounds with unique 2D- and 3D-selenido stannate frameworks. For instance, the use of $(C_4C_1Im)Cl$ and $N_2H_4\cdot H_2O$ led to the formation of a compound with a 3D-$[Sn_9Se_{20}]^{4-}$ structure (Fig. 5(a)), while in $(C_5C_1Im)Cl$ and $N_2H_4\cdot H_2O$, another compound based on a 2D-nanotube-type anion $[Sn_{17}Se_{38}]^{8-}$ (Fig. 5(b)) formed. In the absence of $N_2H_4\cdot H_2O$, nanoparticles were formed instead of single crystals.[96]

Influence of ILs on the packing of identical anions

In certain cases, in which the anionic substructure is extremely thermodynamically favourable, the IL counterions merely control the packing scheme of the latter. This in turn allows to control the spatial separation between discrete cluster or other anionic structural motifs, which also helps in finetuning opto-electronic properties. Additional encapsulation of cations or auxiliary molecules in the anionic part increases the structural diversity of the resulting compounds and influences their stability. A famous example of a mere packing effect was reported for the numerous salts of the $[Sn_{36}Ge_{24}Se_{132}]^{24-}$ anion and a Ge/Sn-disordered analogue: $(C_4C_1C_1Im)_{24}[Sn_{36}Ge_{24}Se_{132}]$ and $(C_4C_1Im)_{24}[Sn_{32.5}Ge_{27.5}Se_{132}]$ were obtained by reacting $K_4[Ge_4Se_{10}]\cdot 3H_2O$ with $SnCl_4\cdot 5H_2O$ in 1:1 mixtures of tetra-fluoridoborate- and chloride-based ILs $(C_4C_1C_1Im)X$ and $(C_4C_1Im)X$ (X = $[BF_4]$, Cl) with the addition of small amounts of 2,6-dimethylmorpholine (DMMP) or without auxiliary amine.

The compounds with the resulting "zeoball" polyanions mentioned above are the largest known discrete main group polyanions with an outer diameter of 11.6 nm and a volume of 820 Å^3 (under consideration of van der Waals radii). The molecular structure of the superspherical "zeoball" cluster anion is shown in Fig. 6(a). Salts comprising the "zeoball" anion have the capacity to capture I_2 molecules and activate I–I bond cleavages to eventually form I_3^-.[97] A series of similar "zeoball" salts with different packing arrangements of cations and anions were obtained by varying the alkyl chain lengths of the 1-alkyl-(2,)3-(di)methylimidazolium cations (alkyl = butyl, hexyl or octyl) used for the synthesis. The nature and size of these cations thus did not affect the formation of the "zeoball" cluster itself, but also impacted the crystal symmetry and packing motifs. Depending on the IL cation selected, more open or more densely packed arrangements emerged. This clearly demonstrated the remarkable thermodynamic stability of the anionic substructure under the given reaction conditions. In addition, however, it also became apparent that the size and shape of the IL cation, as well as their capability to undergo electrostatic interactions and anion$\cdots\pi$ interactions of different strengths, effectively controls the anions' arrangement within the unit cell. Fig. 6(b)–(e) show different crystal packing arrangements of "zeoball" salts.[98] We note in passing that for the reactions to yield this anion, the right choice of the
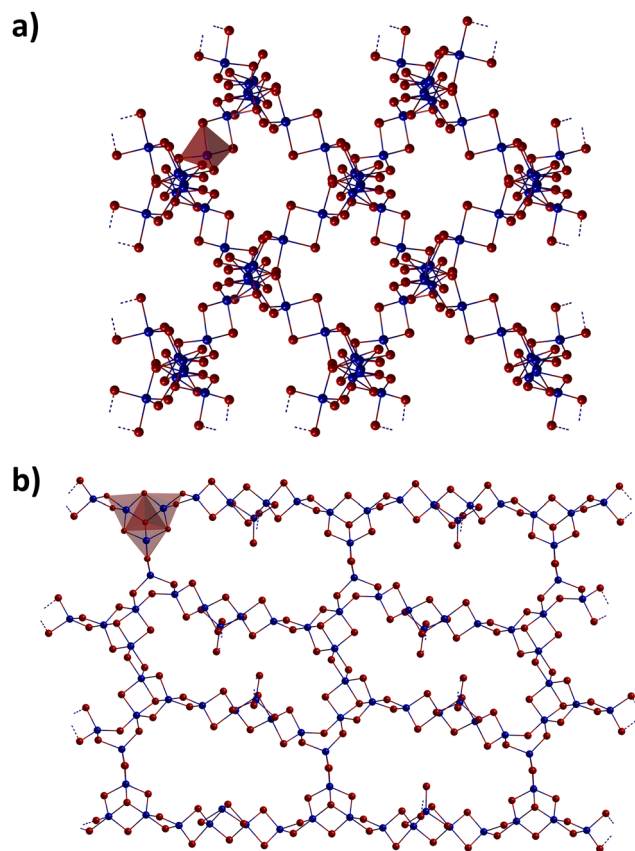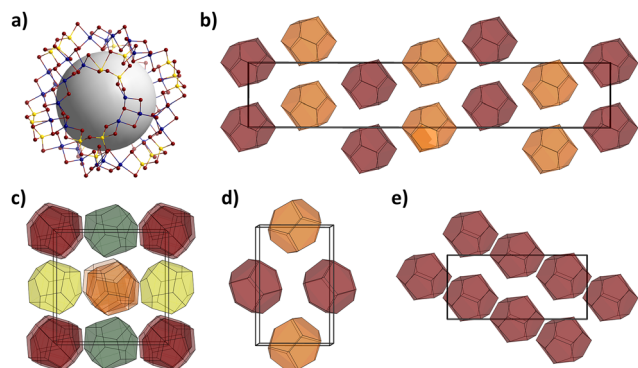

Fig. 5 (a) 3D open-framework of the anion in $(C_4C_1Im)_4[Sn_9Se_{20}]$, and (b) 2D nanotube structure of the anion in $(C_5C_1Im)_8[Sn_{17}Se_{38}]$. Colour code: Sn = dark blue, Se = dark red.

Fig. 6 (a) Molecular structure of the superspherical "zeoball" cluster anion $[Sn_{36}Ge_{24}Se_{132}]^{24-}$, with the grey sphere representing the cavity inside the anion. (b)–(e) Packing patterns of the anions with overall pentagonal dodecahedral topology in different "zeoball" salts. Counterions are omitted for clarity. Colour code: Sn = dark blue, Ge = light orange, Se = dark red.
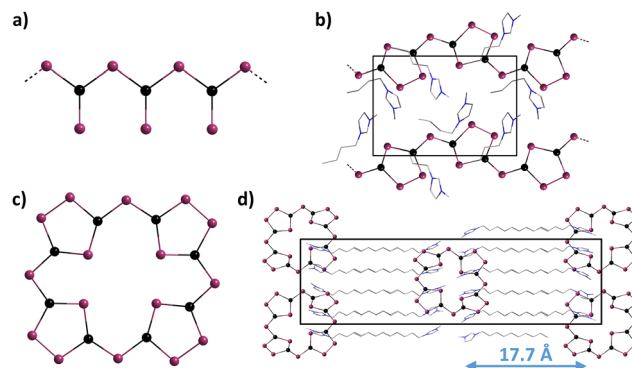
Fig. 7 (a) Anionic structure of $Na_2[HgTe_2]$. (b) Unit cell of $(C_4C_1Im)_2[Hg_2Te_4]$ with the infinite zig-zag-strand of the anion. (c) Anionic substructure of porphyrin-related tellurido mercurate $[Hg_8Te_8(Te_2)_4]^{8-}$. (d) Unit cell of the salt of the latter with $(C_{10}C_1Im)^+$ cations, viewed along the crystallographic a-axis. Colour code: Hg = black, Te = plum, C = grey, N = blue.

IL anion—as a moderator of the metal precursor's reactivity—is instrumental, which is a "normal" effect of the reaction medium, however, and will thus not be discussed here.

The effect of the alkyl chain length on the packing mode was demonstrated even more clearly for tellurido mercurates. The ionothermal treatment of $Na_2[HgTe_2]$, comprising co-planar 1D strands of edge-sharing $\{HgTe_3\}$ triangles (Fig. 7(a)), within the short-chain cation from $(C_4C_1Im)[BF_4]$ yielded $(C_4C_1Im)_2[Hg_2Te_4]$, featuring a novel 1D-type anion. The anion is constituted of $\{Hg_2Te_3\}$ five-membered rings with Te^{2-} and $(Te_2)^{2-}$ ligands (upon partial oxidation of neighbouring Te^{2-} in the precursor), which are connected via additional μ-Te^{2-} bridges (Fig. 7(b)).[99] The structure directing effect of the cations results in crystal structure distinctions when compared with related compounds $\{[Mn(en)_3]_2Cl_2\}$-$[Hg_2Te_4]$ (en = 1,2-diaminoethane) and $\{N(C_2H_5)_4\}_2[Hg_2Te_4]$.[31]

In contrast, the use of ILs with longer alkyl chains $(C_nC_1Im)[BF_4]$ (n = 10, 12) resulted in salts containing the unprecedented molecular anion $[Hg_8Te_{16}]^{8-}$—according to the IL cation effect discussed in the previous section. This inorganic macrocycle also consists of the $\{Hg_2Te(Te_2)\}$ five-membered rings, bridged by Te^{2-} ligands. However, in this case, the result is not a polymeric strand, but a macrocyclic tetramer (Fig. 7(c)). The anion is structurally analogous to organic porphyrins, which consist of four methylene-bridged pyrrole rings. Nevertheless, the total valence electron counts differ significantly (120 in $[Hg_8Te_{16}]^{8-}$ and 114 in porphyrin). $[Hg_8Te_{16}]^{8-}$ is thus not π-aromatic. It is isoelectronic to the $[B_8Ch_{16}]$ structures of BCh_2 (Ch = S, Se),[100] but with the distinction of being charged and significantly deviating from planarity owing to the adoption to the counterion environment, see below (nota bene: isolated molecules in DFT calculations planarize). A cyclic oligomer such as $[Hg_8Te_{16}]^{8-}$ has nor previously been reported. The tendency for the formation of $[Hg_8Te_{16}]^{8-}$ macrocycles over chain-like 1D-$[Hg_2Te_4]^{2-}$ anions can be attributed to the optimal alignment of the molecular anions with the cationic template of the IL. The precise mechanism by which the cyclic $[Hg_8Te_{16}]^{8-}$ is formed remains to be determined; however, it is postulated to

involve a reorganization of the anionic substructure of $Na_2[HgTe_2]$, in addition to (partial) oxidative coupling of the telluride ligands. The formation of dichalcogenide anions in ILs is a relatively facile process, and the ILs appear to be less innocent than initially anticipated, as proven by the observation of a tellurized IL derivative in the complex $[(C_nC_1imTe)_4Hg]^{2+}$.[101] More probably, however, the presence of residual oxygen or components of the IL itself might act as oxidizing agents. A more detailed analysis of the unit cell provides further insights into the structural organisation of the compound. Optimizing the interaction and structural match with the imidazolium cations (also acting as counterions for charge compensation) requires opposite pairs of $\{Hg_2Te(Te_2)\}$ rings to be inclined by approximately $24.8(1)°$. This ensures that the endocyclic Te atoms remain relatively distant from each other ($Te\cdots Te$ distances: $7.0808(7)$– $7.4130(6)$ Å across the centre of the macrocycle).

Further examinations of the crystal structure have revealed a very strict segregation into ionic and non-polar components that, in alternating manner, form a lamellar crystal structure, which is reminiscent of the organization of polar and non-polar components in surfactant-based or lipid-double-layer-based micelles. The non-polar regions are equally the result of van der Waals interactions between the decyl chains, which form a membrane-like interlocked double layer with a width of 17.7 Å that can be widened by extending the chain length to dodecyl, tetradecyl, or hexadecyl. Simultaneously, the positively charged imidazolium rings align precisely with the anions, with two imidazolium rings positioned near each of the four $\{Hg_2Te(Te_2)\}$ units to compensate for the 8– charge of the macrocyclic anions together. In this arrangement, the imidazolium rings are oriented orthogonally to the $\{Hg_2Te(Te_2)\}$ units, thereby maximizing the anion$\cdots$anion distances (Fig. 7(d)).[102] In these examples, ILs clearly influence the formation of novel tellurido mercurate motifs, their assembly into chains or macrocycles, and ultimately, their lamellar arrangement in the crystal.

Other examples showed that the influence of the length of the alkyl chains affect the crystal symmetry of chalcogenido metalates. For instance, the subtle difference of a single

CH$_2$-group in the alkyl chain of imidazolium-based ILs affected the crystal structures of related sulfido stannates. While the use of (C$_4$C$_1$C$_1$Im)Br led to the formation of (C$_4$C$_1$C$_1$Im)$_2$[Sn$_3$S$_7$] with a trigonal crystal structure, the synthesis using (C$_4$C$_1$C$_2$Im)Br resulted in (C$_4$C$_1$C$_2$Im)$_2$[Sn$_3$S$_7$] exhibiting a triclinic crystal structure. The presence of an additional CH$_2$-group in the alkyl chain of the IL leads to steric constraints that distorted the anionic framework. Additional effects include the synthesis temperature. Elevated temperatures at otherwise identical reaction conditions afforded (C$_4$C$_1$C$_2$Im)$_2$[Sn$_4$S$_9$], demonstrating the combined influence of reaction parameters on the product spectrum in these complex ionothermal reactions.[103]

Cooperation of ILs with metal cations

Another study addressed the synergistic structure-directing effects of ILs combined with metal–amine complexes, which were formed *in situ* through various polyamines for the synthesis of novel selenido stannates.

The resulting compounds exhibit diverse anionic structures, including binary 2D layers of [Sn$_3$Se$_7$]$_n^{2n-}$ in (C$_4$C$_1$C$_1$Im)$_3$[Ni(*en*)$_3$]$_2$[Sn$_9$Se$_{21}$]Cl and quasi-ternary 2D layers in (C$_4$C$_1$-Im)$_4$[Ni-(tepa)Cl]$_2$[Ni(tepa)Sn$_{12}$Se$_{28}$] (tepa = tetraethylenepentamine).[104] (C$_4$C$_1$C$_1$Im)$_3$[Ni(*en*)$_3$]$_2$[Sn$_9$Se$_{21}$]Cl features polymeric zig-zag chains of [Sn$_3$Se$_8$]$_n^{4n-}$, formed by {Sn$_3$Se$_{10}$} units linked *via* edge-sharing μ_2-Se atoms along the crystallographic *c*-axis. These chains interconnect through {Sn$_3$Se$_9$} units, creating a lamellar [Sn$_3$Se$_7$]$_n^{2n-}$ structure in the crystallographic *ac*-plane. The structure is defined by eight-membered rings formed by isolated {Sn$_3$Se$_9$} and {Sn$_3$Se$_{10}$} units from neighbouring chains (Fig. 8(a)). Charge-compensating ions, including [Ni(*en*)$_3$]$^{2+}$, (C$_4$C$_1$C$_1$Im)$^+$, and Cl$^-$ are located in the interlamellar spaces, stabilized by extensive hydrogen bonding between the cations, the anionic selenido stannate framework, and Cl$^-$ ions.

The compound (C$_4$C$_1$C$_1$Im)$_4$[Ni(tepa)Cl]$_2$[Ni(tepa)Sn$_{12}$Se$_{28}$] features a layered anionic structure composed of [Sn$_{12}$Se$_{28}$]$^{8-}$ units, which are additionally decorated with [Ni(tepa)]$^{2+}$ complexes through Ni···Se bonds. The layers are constructed from interconnected {Sn$_3$Se$_{10}$} units, forming compressed six-membered rings (Fig. 8(b)). This structural motif is thus different from more prevalent, regular eight-membered rings observed in analogous structures. The [Ni(tepa)]$^{2+}$ complexes are all positioned on the same side of the layers, resulting in a non-centrosymmetric stacking pattern (Fig. 8(c)). The organic cations are intercalated between the layers, contributing to the overall stability of the structure.[104–106] Huang *et al.* also examined the supramolecular interactions in both compounds to better understand the structure-directing behaviour of the ILs. In (C$_4$C$_1$C$_1$Im)$_3$[Ni(*en*)$_3$]$_2$[Sn$_9$Se$_{21}$]Cl, the short C/N···Se/Cl distances and favourable C/N–H···Se/Cl angles indicate the presence of non-classical hydrogen bonding interactions involving the metal–amine complexes, (C$_4$C$_1$C$_1$Im)$^+$ cations, Cl$^-$ anions, and the anionic [Sn$_3$Se$_7$]$_n^{2-}$ layers. Some (C$_4$C$_1$C$_1$Im)$^+$ cations associate with [Ni(*en*)$_3$]$^{2+}$ *via* Cl$^-$ ions, forming cationic complexes that interact with [Sn$_3$Se$_7$]$_n^{2-}$ layers through
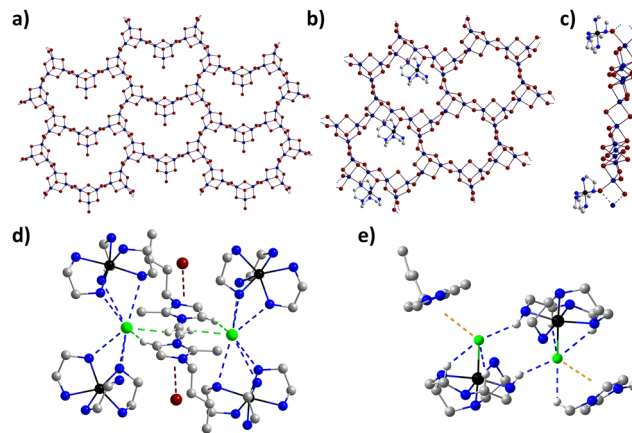
Fig. 8 (a) Eight-membered ring in the binary anionic structure of (C$_4$C$_1$C$_1$Im)$_3$[Ni(*en*)$_3$]$_2$[Sn$_9$Se$_{21}$]Cl, (b) compressed six-membered rings in the quasi-ternary anionic structure of (C$_4$C$_1$C$_1$Im)$_4$[Ni(tepa)Cl]$_2$[Ni(tepa)Sn$_{12}$Se$_{28}$], (c) metal complex-decorated [Ni(tepa)Sn$_{12}$Se$_{28}$]$_n^{6n-}$ layer viewed along the crystallographic *c*-axis. (d) Illustration of H···Cl interactions (blue, dashed) in the cation substructure and with the closest Se atom in (C$_4$C$_1$C$_1$Im)$_3$[Ni(*en*)$_3$]$_2$[Sn$_9$Se$_{21}$]Cl. (e) Illustration of H···Cl (blue, dashed) and anion···π (red, dashed) interactions in the cation substructure. Colour code: Sn = dark blue, Se = dark red, Ni = black, C = grey (tepa) or orange (C$_4$C$_1$C$_1$Im), N = blue, Cl = bright green, H = white.

C/N–H···Se bonds. There are also anion···π interactions between the imidazolium ring of the imidazole rings and the dangling Se atom of the {Sn$_3$Se$_9$} unit. Meanwhile, other (C$_4$C$_1$C$_1$Im)$^+$ cations have been incorporated in the interlamellar space that are directly connected to the [Sn$_3$Se$_7$]$_n^{2n-}$ framework through C–H···Se hydrogen interactions (Fig. 8(d)). The interactions occurring in (C$_4$C$_1$C$_1$Im)$_4$[Ni(tepa)Cl]$_2$[Ni(tepa)Sn$_{12}$Se$_{28}$] are similar to those in (C$_4$C$_1$C$_1$Im)$_3$[Ni(*en*)$_3$]$_2$[Sn$_9$Se$_{21}$]Cl. The two compounds differ in the short C/H···Cl distances (2.28–2.63 Å in (C$_4$C$_1$C$_1$Im)$_3$[Ni(*en*)$_3$]$_2$[Sn$_9$Se$_{21}$]Cl and 2.48–2.81 Å in (C$_4$C$_1$C$_1$Im)$_4$-[Ni(tepa)Cl]$_2$[Ni(tepa)Sn$_{12}$Se$_{28}$]) that indicate the presence of non-classical hydrogen bonding interactions between (C$_4$C$_1$C$_1$Im)$^+$ cations and [Ni(tepa)Cl] moieties.

There are some (C$_4$C$_1$C$_1$Im)$^+$ cations that associate with [Ni(tepa)Cl] *via* Cl$^-$ ions, forming cationic complexes that interact *via* C/N–H···Cl. Furthermore, anion···π interactions occur between the imidazolium ring of the IL cations and Cl$^-$ anions of the [Ni(tepa)Cl] units (Fig. 8(e)). Anion···π interactions between imidazolium cations and halide anions are known to arise from the electrostatic attraction between the negatively charged anion and the electron-deficient π-system of the imidazolium ring.[107,108] The introduction of metal–amine complexes clearly facilitates the formation of aggregated cationic complexes with strong hydrogen interactions, which serve as cooperative SDAs.[109] Additional (C$_4$C$_1$C$_1$Im)$^+$ cations occupy the remaining space to support crystal growth.[104] There are further examples of ILs that were successfully combined with metal–amine complexes. By adjusting the ratio of both components, a new family of selenido stannates featuring the anionic [Sn$_3$Se$_7$]$_n^{2n-}$ layer was obtained, incorporating various types of six- or eight-membered rings.[110]

Imidazolium-based ILs have been the most commonly used media for the ionothermal synthesis of chalcogenido metalate

compounds, owing to their pronounced stability and diversity. Pyridinium-based ILs, such as 1-ethylpyridinium bromide (C_2H_5Py)Br, have received comparatively little attention in this context. However, there are a few examples of their successful application. The choice of the organic backbone of the IL cation for the treatment of Ga, $SnCl_2/Na_2SnO_3$, and Se under otherwise identical reaction conditions was shown to significantly affect the resulting structures. Reactions using the pyridinium-based IL (C_2H_5Py)Br yielded the compound (C_2H_5Py)[$GaSn_2Se_6$]·$1/4H_2O$ with a 3D-open framework where (C_2H_5Py)$^+$ cations reside in the channels of the anionic framework (Fig. 9(a)). In contrast, upon replacement of the pyridinium-based IL by (C_2C_1Im)Br, the product obtained was (C_2C_1Im)$_{1.22}$(NH_4)$_{0.48}$[$Ga_{1.7}Sn_{2.3}Se_8$], which consists of a 3D-framework of pseudo-T4 supertetrahedral clusters following a cubic ZnS-type topology (Fig. 9(b)). A systematic comparison of imidazolium- and pyridinium-based ILs reveals that their structural differences have a significant impact on cluster formation. Imidazolium cations typically promote the condensation of {$GaSe_4$} tetrahedra into supertetrahedral clusters more efficiently, due to their ability to form stronger hydrogen bonds and engage in pronounced anion···π interactions. Pyridinium cations, in contrast, show weaker hydrogen-bonding capabilities and less effective anion···π interactions, both reducing their ability to stabilize supertetrahedral clusters. Furthermore, the limited number of studies on pyridinium-based ILs currently available restricts our understanding of their specific influence on the synthesis of chalcogenido metalates, making it difficult to draw comprehensive conclusions about the relationship between the type of IL and cluster formation. Optical absorption spectra of both compounds suggest that they are semiconductors with band gaps of 2.06 eV for (C_2H_5Py)[$GaSn_2Se_6$]·$1/4H_2O$ and 1.89 eV for (C_2C_1Im)$_{1.22}$(NH_4)$_{0.48}$[$Ga_{1.7}Sn_{2.3}Se_8$] (Fig. 9(c)). The

semiconducting properties inspired an investigation of the compounds' photoelectrochemical performance under visible-light irradiation.

Both materials display n-type semiconductor behaviour, as evidenced by their anodic (positive) photocurrent responses (Fig. 9(d)).[111] The organic backbone of the IL cation hence helped to access significantly different chalcogenido metalate compounds. The reasons for the underlaying differences in the formation procedure are only fragmentarily understood and requires further investigation.

ILs as alkylation agents

Supertetrahedral chalcogenido metalate clusters, a subclass of chalcogenido metalates, are comprised of the following types of clusters: basic-type Tn, penta-type Pn and capped-type C$_{n(,m)}$.[112,113] Within these clusters, Tn-type clusters can be regarded as exact structural fragments of the zinc blende (cubic ZnS) lattice, where n denotes the number of metal layers or metal sites along the tetrahedral edges of the cluster.[114–118]

For many decades, such clusters existed either in their naked versions without any organic attachments, or they were significantly shielded by organic substituents (most commonly attached to the bridging chalcogen atoms) and donor ligands (most commonly coordinating to the metal atoms at the cluster corners). The presence or absence of the organic groups had major influences on solubilities and optical gaps (both increasing massively in the presence of organic groups). It was highly desirable to find a way of attaching only few organic groups to solubilize the clusters without affecting the semiconductor-type optical gap. However, all attempts of a controlled, post-synthetic alkyl or aryl transfer to the clusters by common routes, *e.g.*, using MeI (Me = methyl) or Meerwein's salt,[119,120] had been proven unsuccessful, which was attributed to the low nucleophilicity of the cluster anions, a mismatch of reaction conditions, and solubility issues with the metalate clusters. In 2019, a significant breakthrough was achieved with the formation and isolation of a compound with methylated sulfido-oxido stannate pseudo-T3-supertetrahedra, [$Sn_{10}O_4S_{16}(SMe)_4$]$^{4-}$, which had previously only been observed as purely inorganic, highly-charged anion [$Sn_{10}O_4S_{20}$]$^{8-}$. This development highlighted the safety and potential of ILs in synthetic applications. The reaction temperature and the amount of IL used were key factors in controlling the arrangement of these anionic clusters in their crystalline salts. However, the most important result of this study was the first *in situ* methylation of the terminal sulfide ligands and the first access to a selectively partially methylated chalcogenido metalate cluster. The alkyl group, released from the IL as confirmed by NMR spectroscopy, attacked the cluster structure to form methylthiolate groups at the cluster corners.[121] Notably, this was the first successful post-synthetic alkylation of a chalcogenido metalate cluster, overcoming the previous challenges associated with the conventional (and more toxic) alkylation reagents mentioned above.
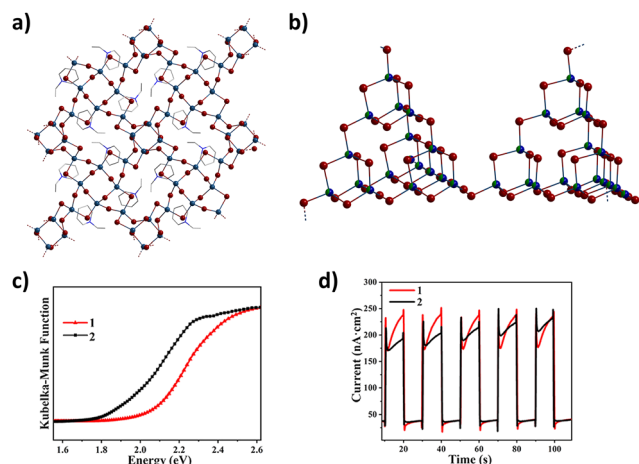
Fig. 9 (a) Crystal structure of the 3D-open-framework compound (C_2H_5Py)[$GaSn_2Se_6$]·$1/4H_2O$. (b) Connection of pseudo-T4 supertetrahedral clusters in the 3D-framework of the anion in (C_2C_1Im)$_{1.22}$(NH_4)$_{0.48}$[$Ga_{1.7}Sn_{2.3}Se_8$]. (c) Solid-state UV-vis spectra and (d) photocurrent responses of (C_2H_5Py)[$GaSn_2Se_6$]·$1/4H_2O$ (1) and (C_2C_1Im)$_{1.22}$(NH_4)$_{0.48}$[$Ga_{1.7}Sn_{2.3}Se_8$] (2). Colour code: Sn/Ga = navy blue, Se = dark red, C = grey, N = blue.

The methylation was not restricted to sulfidooxido stannate supertetrahedra; it was also successfully applied to a P1-type ternary selenido metalate cluster $[Mn_4Sn_4Se_{13}(SeMe)_4]^{6-}$ (Fig. 10(a)) and a tellurido metalate cluster $[Hg_6Te_{10}(TeMe)_2]^{6-}$ under comparable reaction conditions in ILs. This demonstrates the versatility of the method for the selective methylation of terminal chalcogenide ligands.[121]

While the use of ILs with butyl-methyl(-methyl) imidazolium cations of the type $(C_4(C_1)C_1Im)^+$ resulted in selectively methylated products, the approach was recently extended to other alkyl groups (*n*-propyl through *n*-hexyl) by using ILs with symmetrical cation substitution. For instance, reactions with $(C_4C_1C_4Im)Br$ lead to the crystallization of selectively butylated clusters $[Sn_{10}O_4S_{16}(SBu)]^{4-}$ (Bu = butyl) in their respective salts (Fig. 10(b)).[122,123]

The scope of selective functionalization with longer alkyl chains was further expanded through the successful decylation of the tellurido mercurate cluster $[Hg_6Te_{10}(TeDec)_2]^{6-}$ (Dec = decyl), as well as the achievement of an unique heteroleptic functionalization combining methylation and decylation in $[Hg_6Te_{10}(TeDec)(TeMe)]^{6-}$ (Fig. 10(c)). The incorporation of these long alkyl chains at both the cluster and the charge-compensating cations resulted in characteristic lamellar assemblies of cations and anions in the corresponding crystal structures.[124]

Nuclear magnetic resonance (NMR) spectra of the reaction solutions served to prove the IL cations as source for the butyl groups by identifying the released, neutral imidazole molecules (Fig. 11(a)). In contrast to the more highly charged pure inorganic analogous, or to salts of methylated clusters, species that comprise more extended alkyl groups exhibit sufficiently high solubilities in common organic solvents such as CH_3CN. This was confirmed by ^{119}Sn NMR spectroscopy (Fig. 11(b)) and mass spectrometry. Importantly, partial alkylation only leads to minor changes in the electronic structure of the supertetrahedral compounds, so that they maintain their characteristic optoelectronic properties, and all transitions observed in the UV-Vis spectra are of indirect, allowed nature. This opens up new possibilities for functionalizing chalcogenido metalates without
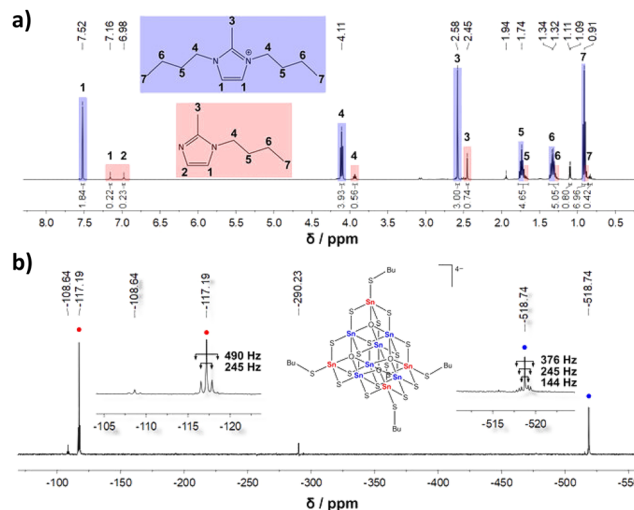

Fig. 11 Identification of the $[Sn_{10}O_4S_{16}(SBu)_4]^{4-}$ cluster in CH_3CN solution using NMR spectroscopy, (a) ^{1}H-NMR spectrum, (b) ^{119}Sn-NMR spectrum with an increased view of the peaks to the two different Sn atomic sites (Sn^A = red, Sn^B = blue). The observed relative intensities do not reflect the actual site population due to the measurement technique. Reproduced with permission from Wiley-VCH.

affecting their physical properties in an undesired way.[122,123] The examples underscore the importance of the role of ILs as effective reagents. The *in situ* alkylation facilitated by ILs highlights their ability to actively participate in chemical transformations. Furthermore, the extension of this method to longer alkyl chains and heteroleptic functionalization highlights the versatility of the ILs' use for tuning solubility and structure properties of the products while preserving the electronic structure of the resulting compounds.

ILs providing donor ligands for metal atoms

ILs have been demonstrated to exhibit dual reactivity in their interactions with terminal chalcogen atoms of chalcogenido metalate clusters. In addition to alkylating these chalcogen atoms (as discussed above), under suitable reaction conditions, they can alternatively replace them entirely. This enhanced versatility significantly broadens the scope for cluster modification, thereby enabling precise control over structural and electronic properties for a wide range of applications.

An example in this context involved the synthesis of four isostructural compounds comprising discrete In-based T3-type clusters, namely $(C_4C_1C_1Im)_5[In_{10}Ch_{16}Cl_3(C_4C_1im)]$ (Ch_{16} = S_{16}; $S_{7.12}Se_{8.88}$; $Se_{13.80}Te_{2.20}$). In these clusters, three of the four In atoms at the corners of the supertetrahedra are coordinated by terminal Cl^- ligands, while the fourth corner exhibits a neutral (C_4C_1im) ligand. Again, the neutral (C_4C_1im) molecule was formed *in situ* from the $(C_4C_1C_1Im)^+$ cation, but in this case is not released into the reaction medium, by used for cluster formation; the Cl^- anions also stemmed from the IL.
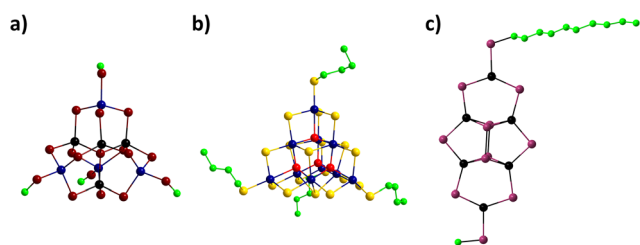
Fig. 10 Molecular structures of (a) the T3-supertetrahedral cluster anion $[Sn_{10}O_4S_{16}(SBu)_4]^{4-}$, selectively butylated at its terminal S atoms, (b) the ternary P1-supertetrahedral cluster anion $[Mn_4Sn_4Se_{13}(SMe)_4]^{6-}$, selectively methylated at its terminal Se atoms, and (c) the cluster anion $[Hg_6Te_{10}(TeDec)(TeMe)]^{6-}$ with a heteroleptic functionalization at its terminal Te atoms combining methylation and decylation. Colour code: Sn = dark blue, Se = dark red, O = red, S = gold, Hg = black, Te = plum, alkyl groups = light green.

The stability of these discrete T3-type clusters is enhanced by reducing the overall negative charge from $-10 = 10 \cdot 3 + 20 \cdot (-2)$ in the T3-cluster $[In_{10}Ch_{20}]^{10-}$ to $-5 = 10 \cdot 3 + 16 \cdot (-2) + 3 \cdot (-1) + 0$ in the modified $[In_{10}Ch_{16}Cl_3(C_4C_1im)]^{5-}$ analogues. Shielding of the cluster corners additionally prevented the Tn clusters from aggregation into open framework structures. (C_4C_1im) groups are good donor ligands that stabilize the isolated T3 clusters by coordinating to corner In atoms. At the same time, this coordination effectively prevents the clusters from further aggregation, as the (C_4C_1im) groups are unable to form bridges. The organic ligand further reduces the overall polarity of the T3 cluster unit, which appears to contribute to the preference of the molecular form, too. As usual, the surrounding $(C_4C_1C_1Im)^+$ cations were shown to contribute to the stabilization, primarily through the facilitation of significant anion···π interactions between the chalcogen atoms and the imidazole rings. The latter are aligned parallel to the tetrahedral faces of the cluster, with the shortest observed distance being 3.2845(5) Å. It is noteworthy that the T3-type indium selenide or telluride clusters. By adjusting the elemental ratio of S:Se:Te, the absorption energies could be fine-tuned from the UV to the visible spectrum, allowing precise control of the photodegradation activity towards methyl orange.[125] In addition, slight modification of the reaction conditions allowed for the replacement of the imidazole ligands with chloride ions, resulting in the formation of $(C_4C_1C_1Im)_6$ $[In_{10}Se_{16}Cl_4](C_1im)_2$. In the presence of DMSO (DMSO = dimethylsulfoxide) these organic-ligand free clusters could be dispersed and degraded into nanoparticles. These nanoparticles exhibited superior photocatalytic H_2 evolution activity in comparison to the original crystals (with organic-ligands).[126]

The substitution of terminal chalcogen atoms by components of the IL used is not limited to the T3-type clusters presented above; it has also been observed in T4 to T6 clusters. This replacement occurs through the process of aliovalent incorporation of M^+ (*e.g.*, Cu^+) or M^{2+} (*e.g.*, Zn^{2+}, Cd^{2+}, Mn^{2+}).[113] For instance, the synthesis of T5-supertetrahedral chalcogenido metalate clusters with a ternary M–In–Ch composition (M = Cu, Cd; Ch = Se, S/Se) has been demonstrated. It is noteworthy that these clusters represent the first discrete inorganic–organic T5-supertetrahedral clusters and that they were shown to exhibit promising photoluminescence properties. The four vertex positions of the T5 core of $[Cd_6In_{28}Ch_{52}Cl_3(C_1im)]^{12-}$ ($Ch_{52} = Se_{52}$; $Se_{28.5}S_{23.5}$; $Se_{16}S_{36}$) are occupied by one (C_1im) and three Cl^- ligands. As mentioned above, these ligands are crucial for the stabilization and formation of discrete clusters. The terminal In–Cl and In–N bonds at the vertices provide a lower overall negative charge compared to M–Ch bonds, which helps prevent polymerization. Furthermore, the crystallization of the compound with the $[Cd_6In_{28}Se_8 S_{44}Cl(C_1im)_3]^{9-}$ ion demonstrated the possibility of ligand modification. Previously, all clusters had three Cl^- and one organic ligand, but variations in the synthesis methods lead to the incorporation of three organic ligands while retaining only one Cl^- ligand. When Cd^{2+} was replaced with Cu^+, a series of compounds based on Cu–In–Ch clusters with different Se:S

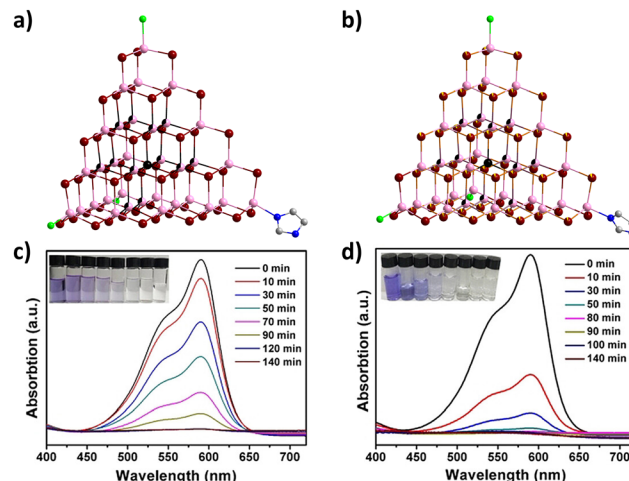Fig. 12 Molecular structure of (a) $[Cu_5In_{30}Se_{52}Cl_3(im)]^{12-}$ and (b) $[Cu_5In_{30}-Se_{48.5}S_{3.5}Cl_3(im)]^{12-}$. Photodegradation of crystal violet in the presence of single crystals of (c) $(C_4C_1Im)_{12}[Cu_5In_{30}Se_{52}Cl_3(im)]$ and (d) $(C_4C_1Im)_{12}[Cu_5In_{30}-Se_{48.5}S_{3.5}Cl_3(im)]$ under visible-light irradiation monitored by diffuse reflectance spectroscopy. Colour code: In = rose, Cd = black, Se = dark red, Cl = bright green, C = grey, N = blue.

ratios were synthesized, namely $[Cu_5In_{30}Ch_{52}Cl_3(im)]^{12-}$ ($Ch_{52} = Se_{52}$; $Se_{48.5}S_{3.5}$; Fig. 12(a) and (b)). Here, imidazole was formed upon removal of all substituents from $(C_4C_1C_1Im)^+$, while in the examples discussed above, (C_4C_1im) or (C_1im) were retained.

Photocatalytic studies indicated that Cu–In–Ch clusters are effective for the degradation of organic dyes under visible light, while Cd–In–Ch clusters exhibited enhanced H_2 evolution activity, with higher S content correlating with increased efficiency (Fig. 12(c) and (d)). These experiments were conducted in a closed glass circulation system with distilled water, triethanolamine, $H_2[PtCl_4]$, and the solid sample under Xe lamp irradiation ($\lambda > 420$ nm). The generated H_2 was quantified by gas chromatography. These modifications highlight the versatility of cluster design in and with ILs.[127] Beyond In-based clusters, the substitution of In^{3+} by Ga^{3+} has led to the formation of a series of T5-cluster, $(C_4C_1C_1Im)_{10}(NH_4)_3[Cu_5-Ga_{30}S_{52}(SH)_4]$, $(C_4C_1C_1Im)_8(NH_4)_2[Cu_5Ga_{30}S_{52}(SH)_2(C_4im)_2]$, and $(C_4C_1C_1Im)_{9.5}(NH_4)_2[Cu_5Ga_{30}S_{52}-(SH)_{1.5}Cl(C_4im)_{1.5}]$ (Fig. 13). These compounds, synthesized in $(C_4C_1C_1Im)Cl$, exhibit the same
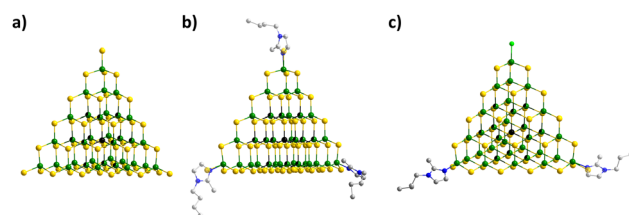
Fig. 13 Discrete T5-clusters (a) $[Cu_5Ga_{30}S_{52}(SH)_4]^{13-}$ in $(C_4C_1C_1Im)_{10}-(NH_4)_3[Cu_5Ga_{30}S_{52}(SH)_4]$, (b) $[Cu_5Ga_{30}S_{52}(SH)_2(C_4im)_2]^{11-}$ in $(C_4C_1C_1Im)_8-(NH_4)_2[Cu_5Ga_{30}S_{52}(SH)_2(C_4im)_2]$ and (c) $[Cu_5Ga_{30}S_{52}(SH)_{1.5}Cl(C_4im)_{1.5}]^{11.5-}$ in $(C_4C_1C_1Im)_{9.5}(NH_4)_2[Cu_5Ga_{30}S_{52}(SH)_{1.5}Cl(C_4im)_{1.5}]$. Organic counterions are omitted for clarity. Colour code: Ga = green, Cu = black, S = gold, C = grey, N = blue.

T5-cluster core $\{Cu_5Ga_{30}S_{52}\}$, while the structures differ in the modification of the cluster corners exhibiting Cl^-, SH^-, or *in situ*-generated (C_4C_1im). The hybrid organic–inorganic compounds show broad photoluminescence emission from 500 to 800 nm, with the full width at half maximum being approximately 180 nm.[128]

Notably, in all examples mentioned above that involve the *in situ* decomposition of IL cations, the IL assumes at least a twofold non-innocent behaviour: the cations turn into neutral imidazole molecules, that (along with Cl^- anions from the IL) serve to terminate the supertetrahedra, or alternatively, the alkyl groups released are transferred to the cluster corners. In addition, the unaltered Im cations act as counterions with their discussed crucial role in structure formation and crystallization.

Polycationic chalcogenide compounds

The discussions in this feature article have so far been limited to cases where the cations of ILs, but not the anions, are incorporated into the final structures of crystalline chalcogenido metalates. However, polycationic chalcogenide compounds provide compelling evidence that the anions of ILs can also be directly incorporated and as such affect the product structures and properties.

The first breakthrough in this specific field was reported by Kanatzidis *et al.* with the synthesis of the polycationic species $[Sb_7S_8Br_2]^{3+}$ in a Lewis acidic IL medium consisting of $(C_2C_1Im)Br$ and $AlCl_3$. The cation features interconnected heterocubane-type $\{Sb_2S_2\}$ units, which are further coordinated by bromide ligands derived from the IL (Fig. 14(a) and (b)). The compound has an optical band gap of 2.03 eV (Fig. 14(c)) and exhibits non-linear optical properties due to its non-centrosymmetric structure. This enables its application for
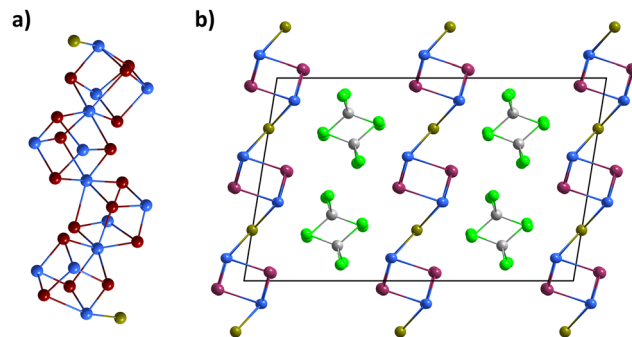
Fig. 14 (a) Molecular Structure of the polycationic unit $[Sb_7S_8Br_2]^{3+}$. (b) Packing of the polycations and $[AlCl_4]^-$ anions in the (extended) unit cell of $[Sb_7S_8Br_2][AlCl_4]_3$. (c) Absorption spectrum of single crystals of $[Sb_7S_8Br_2][AlCl_4]_3$. (d) Second harmonic generation of $[Sb_7S_8Br_2][AlCl_4]_3$ compared to the benchmark material KH_2PO_4 (KDP). Panels (c) and (d) reproduces with permission from ACS. Colour code: Sn = dark blue, Se = dark red. Sb = light blue, S = gold, Br = dark yellow.

Fig. 15 (a) Structure of the largest known molecular main group metal polycation $[Sb_{13}Se_{16}Br_2]^{5+}$. (b) Packing in the unit cell of $[Bi_2Te_2Br][AlCl_4]$. Colour code: Sb = light blue, Se = dark red, Br = dark yellow, Al = light grey, Cl = bright green.

second harmonic generation (SHG, Fig. 14(d)) and differential frequency generation.[129]

Following this discovery, the use of the bromide-rich IL $(C_4C_1Im)Br/AlBr_3$ led to the formation of $[Sb_{13}Se_{16}Br_2][Sb_7Se_8Br_2]$-$[AlBr_4]_8$, a formal double salt of two polycationic units. The $[Sb_{13}Se_{16}Br_2]^{5+}$ cation represents the largest known molecular main group metal polycation composed of four heterocubane units, with bromide ligands terminating the outermost Sb atoms (Fig. 15(a)). The crystal structure of the $[Sb_7Se_8Br_2]^{3+}$ salt is analogous to that of the sulfur compound mentioned above.[130]

In addition to the successful synthesis of discrete polycationic species, layered polycationic chalcohalide compounds have also been realized. Kanatzidis *et al.* reported an isostructural class of such materials, including 2D-$[Bi_2Te_2Br][AlCl_4]$, 2D-$[Sb_2Te_2Br][AlCl_4]$ and 2D-$[Bi_2Se_2Br][AlCl_4]$. The layered 2D-$[Bi_2Te_2Br]^+$ cation consists of interconnected $\{Bi_2Te_2\}$ rings forming extended layers by bridging Br atoms. The incorporation of $[AlCl_4]^-$ anions from the reaction medium provides charge neutrality and structural stabilization through the isotropic, near spherical anion (Fig. 15(b)). Notably, $[Bi_2Te_2Br]$-$[AlCl_4]$ exhibits a strongly anisotropic behaviour, as evidenced by optical and electrical measurements as well as theoretical calculations of its electronic band structure and density of states.[131,132] The capacity of ILs to incorporate Lewis acids introduces new opportunities for the synthesis of cationic species, diverging from the anionic compounds typically obtained in molten salts chemistry.[129]

Further aspects

This article alluded to the capacity of ILs to interact and react with the substrates and become an integral part of the reaction products. It did not cover all parameters that control the role of ILs as reaction media—most of them have simply not been investigated in a systematic way to date. However, in this section, we briefly refer to additional factors that influence the reaction behaviour of ILs in order to illustrate the breadth and complexity of the reaction space that are provided by them. One of these factors is the ability of ILs to dissolve the reactants at all, which depends on their polarity, which in turn is defined
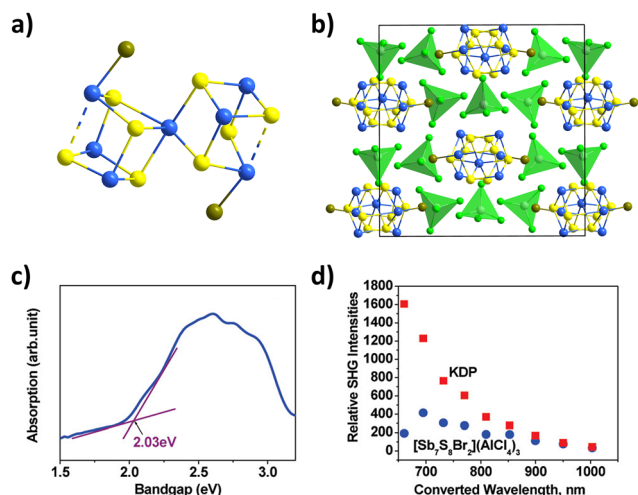
by the composition and charge of the ions involved. A direct consequence of this property is the resulting concentration of the reactants, which significantly influences the kinetics of the ongoing reactions. As another consequence of the concentration of reactants and (commonly basic) additives, the reaction medium will adopt a certain pH value that also plays a decisive role—particularly in regards of framework formation by help of hydrogen bonding interactions. There is a lack of precise information on all these factors. This is largely due to the fact that it is not trivial to survey and monitor the reactions, which are usually carried out in small volumes and in sealed ampoules or autoclaves within an oven. Future experimental setups should be designed in a way that allows for such studies though. A more comprehensive understanding of all the parameters involved in the reaction will eventually enable tailor-made reactions for the design and development of new materials in a more targeted manner.

Conclusions

The role of ILs in the synthesis of chalcogenido metalates goes beyond their traditional role as reaction media. Their non-innocent behaviour actively influences the formation, stabilization, and functionalisation of the desired materials, providing an additional level of synthetic influence and control. By acting as charge-balancing counterions, providers of anion$\cdots\pi$ interaction, and structural stabilizer, ILs enable the formation of discrete clusters that would otherwise be difficult to isolate. Additionally, their ability to participate in specific transformations—such as selective alkylation of terminal chalcogenide positions or ligand-exchange reactions at metal coordination sites—opens up new synthetic pathways, particularly in the context of post-synthetic modification, and thereby provides an additional means of fine-tuning.

Beyond their role in tailoring cluster formation, ILs thus significantly influence materials properties by controlling solubility, optical absorption and electronic conductivity. Besides charge balance and spatial separation, ILs prevent unwanted aggregation while promoting the formation of well-defined, discrete clusters with distinct structural and electronic properties.

Their overall function as structure-directing agents, charge-compensating counterions and even reactive species broadens the scope of cluster engineering and allows the design of functional materials.

In summary, this feature article highlighted the significant impact of non-innocent ILs on the development of novel functional materials and underlined the need for continued research to fully realise the versatility of ILs in the synthesis and post-synthetic modification of chalcogenido metalate compounds.

Author contributions

All authors co-wrote the article.

Conflicts of interest

There are no conflicts to declare.

Data availability

No primary research results, software or code have been included and no new data were generated or analysed as part of this review.

Acknowledgements

Notes and references

1 J. H. MacNeil, D. M. Massi, J.-H. Zhang, K. A. Rosmus, C. D. Brunetta, T. A. Gentile and J. A. Aitken, *J. Alloys Compd.*, 2014, **586**, 736–744.
2 T. Kaib, S. Haddadpour, H. F. Andersen, L. Mayrhofer, T. T. Järvi, M. Moseler, K.-C. Möller and S. Dehnen, *Adv. Funct. Mater.*, 2013, **23**, 5693–5699.
3 M. Hao, Q. Hu, Y. Zhang, M. Luo, Y. Wang, B. Hu, J. Li and X. Huang, *Inorg. Chem.*, 2019, **58**, 5126–5133.
4 J. Zander and R. Marschall, *J. Mater. Chem. A*, 2023, **11**, 17066–17078.
5 N. Zheng, X. Bu, B. Wang and P. Feng, *Science*, 2002, **298**, 2366–2369.
6 A. Benkada, H. Reinsch, M. Poschmann, J. Krahmer, N. Pienack and W. Bensch, *Inorg. Chem.*, 2019, **58**, 2354–2362.
7 N. Pienack, A. Puls, C. Näther and W. Bensch, *Inorg. Chem.*, 2008, **47**, 9606–9611.
8 N. Zheng, X. Bu, H. Vu and P. Feng, *Angew. Chem., Int. Ed.*, 2005, **44**, 5299–5303.
9 S. Saha, G. Das, J. Thote and R. Banerjee, *J. Am. Chem. Soc.*, 2014, **136**, 14845–14851.
10 Q. Zhang, I. Chung, J. I. Jang, J. B. Ketterson and M. G. Kanatzidis, *J. Am. Chem. Soc.*, 2009, **131**, 9896–9897.
11 Z.-Z. Luo, C.-S. Lin, W.-D. Cheng, H. Zhang, W.-L. Zhang and Z.-Z. He, *Inorg. Chem.*, 2013, **52**, 273–279.
12 J. He, Y. Guo, W. Huang, X. Zhang, J. Yao, T. Zhai and F. Huang, *Inorg. Chem.*, 2018, **57**, 9918–9924.
13 A. K. Iyer, J. B. Cho, M. J. Waters, J. S. Cho, B. M. Oxley, J. M. Rondinelli, J. I. Jang and M. G. Kanatzidis, *Chem. Mater.*, 2022, **34**, 5283–5293.
14 M. J. Manos and M. G. Kanatzidis, *Chem. Sci.*, 2016, **7**, 4804–4824.
15 H.-W. Liu, K.-Y. Wang, D. Ding, M. Sun, L. Cheng and C. Wang, *Chem. Commun.*, 2019, **55**, 13884–13887.
16 M. A. Quintero, A. D. Pournara, R. Godsel, Z. Li, S. Panuganti, X. Zhou, C. Wolverton and M. G. Kanatzidis, *Inorg. Chem.*, 2023, **62**, 15971–15982.
17 I. U. Arachchige, G. S. Armatas, K. Biswas, K. S. Subrahmanyam, S. Latturner, C. D. Malliakas, M. J. Manos, Y. Oh, K. Polychronopoulou, P. F. P. Poudeu, P. N. Trikalitis, Q. Zhang, L.-D. Zhao and S. C. Peter, *Inorg. Chem.*, 2017, **56**, 7582–7597.
18 A. V. Bhaskar Reddy, M. Moniruzzaman, M. A. Bustam, M. Goto, B. B. Saha and C. Janiak, *J. Mater. Chem. A*, 2020, **8**, 15034–15041.
19 Q.-Y. Zhu and J. Dai, *Coord. Chem. Rev.*, 2017, **330**, 95–109.
20 G.-N. Liu, G.-C. Guo, F. Chen, S.-H. Wang, J. Sun and J.-S. Huang, *Inorg. Chem.*, 2012, **51**, 472–482.
21 J.-M. Yu, D. Luo, Z.-J. Ma, B. Zheng, F.-F. Cheng and W.-W. Xiong, *ACS Appl. Mater. Interfaces*, 2021, **13**, 55188–55197.
22 Z. Wu, G. Stuhrmann and S. Dehnen, *Chem. Commun.*, 2022, **58**, 11609–11624.

23 D. Freudenmann, S. Wolf, M. Wolff and C. Feldmann, *Angew. Chem., Int. Ed.*, 2011, **50**, 11050–11060.

24 M. G. Kanatzidis, *Inorg. Chem.*, 2017, **56**, 3158–3173.

25 S. Santner, J. Heine and S. Dehnen, *Angew. Chem., Int. Ed.*, 2016, **55**, 876–893.

26 X. Zhou, V. S. C. Kolluru, W. Xu, L. Wang, T. Chang, Y.-S. Chen, L. Yu, J. Wen, M. K. Y. Chan, D. Y. Chung and M. G. Kanatzidis, *Nature*, 2022, **612**, 72–77.

27 T. Eisa, M. A. Abdelkareem, D. A. Jadhav, H. O. Mohamed, E. T. Sayed, A. G. Olabi, P. Castaño and K.-J. Chae, *Prog. Energy Combust. Sci.*, 2023, **94**, 101044.

28 J. D. Martin, A. M. Dattelbaum, T. A. Thornton, R. M. Sullivan, J. Yang and M. T. Peachey, *Chem. Mater.*, 1998, **10**, 2699–2713.

29 Y.-J. Lu and J. A. Ibers, *Comments Inorg. Chem.*, 1993, **14**, 229–243.

30 W. S. Sheldrick and M. Wachhold, *Angew. Chem., Int. Ed. Engl.*, 1997, **109**, 214–234.

31 S. S. Dhingra, C. J. Warren, R. C. Haushalter and A. B. Bocarsly, *Chem. Mater.*, 1994, **6**, 2382–2385.

32 M. G. Kanatzidis, *Chem. Mater.*, 1990, **2**, 353–363.

33 K. Chondroudis and M. G. Kanatzidis, *Inorg. Chem.*, 1995, **34**, 5401–5402.

34 S. E. Latturner, *Acc. Chem. Res.*, 2018, **51**, 40–48.

35 G. Thiele, P. Bron, S. Lippert, F. Nietschke, O. Oeckler, M. Koch, B. Roling and S. Dehnen, *Inorg. Chem.*, 2019, **58**, 4052–4054.

36 E. Ruzin, S. Jakobi and S. Dehnen, *Z. Anorg. Allg. Chem.*, 2008, **634**, 995–1001.

37 C. Zimmermann, C. E. Anson, F. Weigend, R. Clérac and S. Dehnen, *Inorg. Chem.*, 2005, **44**, 5686–5695.

38 E. Ruzin, A. Fuchs and S. Dehnen, *Chem. Commun.*, 2006, 4796–4798.

39 G. Demazeau, *J. Mater. Sci.*, 2008, **43**, 2104–2114.

40 M. H. Mruthunjayappa, N. S. Kotrappanavar and D. Mondal, *Prog. Mater. Sci.*, 2022, **126**, 100932.

41 C. Cui, H. Pan, L. Wang and M. Baiyin, *Cryst. Growth Des.*, 2024, **24**, 1227–1234.

42 G. Thiele, S. Santner, C. Donsbach, M. Assmann, M. Müller and S. Dehnen, *Z. Kristallogr. – Cryst. Mater.*, 2014, **229**, 489–495.

43 T. Richter and R. Niewa, *Inorganics*, 2014, **2**, 29–78.

44 J. Guo, H. Lei, F. Hayashi and H. Hosono, *Nat. Commun.*, 2014, **5**, 4756.

45 S. Li, J. Han, L. Zhang, W. Jiang and D. Jia, *J. Solid State Chem.*, 2019, **269**, 341–347.

46 J. Han, S. Li, C. Tang, W. Zheng, W. Jiang and D. Jia, *RSC Adv.*, 2018, **8**, 34078–34087.

47 J. A. Cody, K. B. Finch, G. J. Reynders, G. C. B. Alexander, H. G. Lim, C. Näther and W. Bensch, *Inorg. Chem.*, 2012, **51**, 13357–13362.

48 K. Ghandi, *Green Sustain. Chem.*, 2014, **04**, 44–53.

49 T. Niu, L. Chao, W. Gao, C. Ran, L. Song, Y. Chen, L. Fu and W. Huang, *ACS Energy Lett.*, 2021, 1453–1479.

50 L. Nie, Y. Zhang, W.-W. Xiong, T.-T. Lim, R. Xu, Q. Yan and Q. Zhang, *Inorg. Chem. Front.*, 2016, **3**, 111–116.

51 S. K. Singh and A. W. Savoy, *J. Mol. Liq.*, 2020, **297**, 112038.

52 P. Wasserscheid and T. Welton, *Ionic liquids in synthesis*, Wiley-VCH, Weinheim, 2nd completely revised and enlarged edn, 2008.

53 P. T. Anastas, *Green Solvents: Ionic Liquids*, John Wiley & Sons, Incorporated, Weinheim, 1st edn, 2013.

54 P. I. Walden, *Bull Acad Imper Sci*, 1914, 405–422.

55 R. M. Barrer, *Trans. Faraday Soc.*, 1943, **39**, 59.

56 A. P. De Los Ríos, A. Irabien, F. Hollmann and F. J. H. Fernández, *J. Chem.*, 2013, **2013**, 402172.

57 D. Valli Sowbhagyam, *Int. Res. J. Adv. Eng. Hub.*, 2024, **2**, 220–224.

58 A. S. Wells and V. T. Coombe, *Org. Process Res. Dev.*, 2006, **10**, 794–798.

59 N. Kaur, V. S. Mithu and S. Kumar, *J. Mol. Liq.*, 2024, **397**, 124095.

60 T. P. Thuy Pham, C.-W. Cho and Y.-S. Yun, *Water Res.*, 2010, **44**, 352–372.

61 N. V. Plechkova and K. R. Seddon, in *Methods and Reagents for Green Chemistry*, ed. P. Tundo, A. Perosa and F. Zecchini, Wiley, 1st edn, 2007, pp. 103–130.

62 T. Zhang, T. Doert, H. Wang, S. Zhang and M. Ruck, *Angew. Chem., Int. Ed.*, 2021, **60**, 22148–22165.

63 M. J. Earle and K. R. Seddon, *Pure Appl. Chem.*, 2000, **72**, 1391–1398.

64 Y. Zhou, *Curr. Nanosci.*, 2005, **1**, 35–42.

65 A. Taubert and Z. Li, *Dalton Trans.*, 2007, 723–727.

66 Z. Ma, J. Yu and S. Dai, *Adv. Mater.*, 2010, **22**, 261–285.

67 N. Fechler, T. Fellinger and M. Antonietti, *Adv. Mater.*, 2013, **25**, 75–79.

68 K. Z. Donato, R. K. Donato, M. Lavorgna, L. Ambrosio, L. Matějka, R. S. Mauler and H. S. Schrekker, *J. Sol-Gel Sci. Technol.*, 2015, **76**, 414–427.

69 S. Zhang, K. Dokko and M. Watanabe, *Mater. Horiz.*, 2015, **2**, 168–197.

70 H. Xing, F. Yu, X. Li, Y. Bao, W. Ye, C. Li, S. Zheng and M. Huang, *Sep. Purif. Technol.*, 2025, **360**, 130981.

71 X. Hu, Y. Wang, X. Feng, L. Wang, M. Ouyang and Q. Zhang, *Renewable Sustainable Energy Rev.*, 2025, **207**, 114949.

72 K. Matuszek, S. L. Piper, A. Brzęczek-Szafran, B. Roy, S. Saher, J. M. Pringle and D. R. MacFarlane, *Adv. Mater.*, 2024, **36**, 2313023.

73 J. Lian, T. Kim, X. Liu, J. Ma and W. Zheng, *J. Phys. Chem. C*, 2009, **113**, 9135–9140.

74 D. Tan, F. Wang, T. Pietsch, M. A. Grasser, T. Doert and M. Ruck, *ACS Appl. Energy Mater.*, 2019, **2**, 5140–5145.

75 D. Tan, B. Kirbus, L. M. Eng and M. Ruck, *Eur. J. Inorg. Chem.*, 2020, 2465–2469.

76 S. Arlt, K. Bläsing, J. Harloff, K. C. Laatz, D. Michalik, S. Nier, A. Schulz, P. Stoer, A. Stoffers and A. Villinger, *ChemistryOpen*, 2021, **10**, 62–71.

77 S. Arlt, K. Bläsing, J. Harloff, K. C. Laatz, D. Michalik, S. Nier, A. Schulz, P. Stoer, A. Stoffers and A. Villinger, *ChemistryOpen*, 2021, **10**, 62–71.

78 P. A. Smith and P. C. Burns, *CrystEngComm*, 2014, **16**, 7244–7250.

79 X. Meng and F.-S. Xiao, *Chem. Rev.*, 2014, **114**, 1521–1543.

80 M. A. Grasser, T. Pietsch, E. Brunner, T. Doert and M. Ruck, *ChemistryOpen*, 2021, **10**, 117–124.

81 S. Sowmiah, V. Srinivasadesikan, M.-C. Tseng and Y.-H. Chu, *Molecules*, 2009, **14**, 3780–3813.

82 M. G. Del Pópolo and G. A. Voth, *J. Phys. Chem. B*, 2004, **108**, 1744–1752.

83 A. Stoppa, J. Hunger, R. Buchner, G. Hefter, A. Thoman and H. Helm, *J. Phys. Chem. B*, 2008, **112**, 4854–4858.

84 A. Wulf, K. Fumino and R. Ludwig, *J. Phys. Chem. A*, 2010, **114**, 685–686.

85 S. Men, Y. Jin and P. Licence, *Phys. Chem. Chem. Phys.*, 2020, **22**, 17394–17400.

86 E. Gousseva, F. K. Towers Tompkins, J. M. Seymour, L. G. Parker, C. J. Clarke, R. G. Palgrave, R. A. Bennett, R. Grau-Crespo and K. R. J. Lovelock, *J. Phys. Chem. B*, 2024, **128**, 5030–5043.

87 R. Rowe, K. R. J. Lovelock and P. A. Hunt, *J. Chem. Phys.*, 2021, **155**, 014501.

88 Y. Lin, W. Massa and S. Dehnen, *Chem. – Eur. J.*, 2012, **18**, 13427–13434.

89 Y. Lin and S. Dehnen, *Inorg. Chem.*, 2011, **50**, 7913–7915.

90 Y. Lin, D. Xie, W. Massa, L. Mayrhofer, S. Lippert, B. Ewers, A. Chernikov, M. Koch and S. Dehnen, *Chem. – Eur. J.*, 2013, **19**, 8806–8813.

91 J.-R. Li, W.-W. Xiong, Z.-L. Xie, C.-F. Du, G.-D. Zou and X.-Y. Huang, *Chem. Commun.*, 2013, **49**, 181–183.

92 Z. Wu, I. Nußbruch, S. Nier and S. Dehnen, *JACS Au*, 2022, **2**, 204–213.

93 R. Elfgen, O. Hollóczki and B. Kirchner, *Acc. Chem. Res.*, 2017, **50**, 2949–2957.

94 E. R. Parnham and R. E. Morris, *Acc. Chem. Res.*, 2007, **40**, 1005–1013.

95 E. R. Cooper, C. D. Andrews, P. S. Wheatley, P. B. Webb, P. Wormald and R. E. Morris, *Nature*, 2004, **430**, 1012–1016.

96 J.-R. Li, Z.-L. Xie, X.-W. He, L.-H. Li and X.-Y. Huang, *Angew. Chem., Int. Ed.*, 2011, **50**, 11395–11399.

97 Y. Lin, W. Massa and S. Dehnen, *J. Am. Chem. Soc.*, 2012, **134**, 4497–4500.

98 S. Santner, S. Yogendra, J. J. Weigand and S. Dehnen, *Chem. – Eur. J.*, 2017, **23**, 1999–2004.

99 C. Donsbach and S. Dehnen, *Z. Anorg. Allg. Chem.*, 2017, **643**, 14–19.

100 B. Krebs and H.-U. Hürter, *Angew. Chem., Int. Ed. Engl.*, 1980, **92**, 479–480.

101 C. Donsbach and S. Dehnen, *Eur. J. Inorg. Chem.*, 2018, 4429–4433.

102 C. Donsbach, K. Reiter, D. Sundholm, F. Weigend and S. Dehnen, *Angew. Chem., Int. Ed.*, 2018, **57**, 8770–8774.

103 B. Peters, M. Möbs, N. Michel, F. Tambornino and S. Dehnen, *ChemistryOpen*, 2021, **10**, 227–232.

104 C.-F. Du, N.-N. Shen, J.-R. Li, M.-T. Hao, Z. Wang and X.-Y. Huang, *Chem. – Asian J.*, 2016, **11**, 1555–1564.

105 D. Hinchcliffe, A. Dodd, A. Schmidt and P. Nockemann, *Comprehensive Coordination Chemistry III*, Elsevier, 2021, pp. 557–589.

106 K.-Y. Wang, H.-W. Liu, S. Zhang, D. Ding, L. Cheng and C. Wang, *Inorg. Chem.*, 2019, **58**, 2942–2953.

107 J. D. Holbrey, W. M. Reichert, M. Nieuwenhuyzen, O. Sheppard, C. Hardacre and R. D. Rogers, *Chem. Commun.*, 2003, 476–477.

108 R. Xu, W. Zhang, J. Guan, Y. Xu, L. Wang, H. Ma, Z. Tian, X. Han, L. Lin and X. Bao, *Chem. – Eur. J.*, 2009, **15**, 5348–5354.

109 L. Leclercq and A. R. Schmitzer, *Supramol. Chem.*, 2009, **21**, 245–263.

110 C.-F. Du, J.-R. Li, M.-L. Feng, G.-D. Zou, N.-N. Shen and X.-Y. Huang, *Dalton Trans.*, 2015, **44**, 7364–7372.

111 J.-M. Yu, J.-P. Yu, N. Wang, L.-L. Xiao, H. Wang, Q. Xu, B. Zheng, F.-F. Cheng and W.-W. Xiong, *Inorg. Chem.*, 2021, **60**, 4337–4341.

112 Z. Wu, M. Tallu, G. Stuhrmann and S. Dehnen, *Coord. Chem. Rev.*, 2023, **497**, 215424.

113 X. Bu, N. Zheng and P. Feng, *Chem. – Eur. J.*, 2004, **10**, 3356–3362.

114 H. Li, A. Laine, M. O'Keeffe and O. M. Yaghi, *Science*, 1999, **283**, 1145–1147.

115 G. S. H. Lee, D. C. Craig, I. Ma, M. L. Scudder, T. D. Bailey and I. G. Dance, *J. Am. Chem. Soc.*, 1988, **110**, 4863–4864.

116 P. Feng, X. Bu and N. Zheng, *Acc. Chem. Res.*, 2005, **38**, 293–303.

117 S. Dehnen, *Clusters-contemporary insight in structure and bonding*, Springer, Cham, 2017.

118 T. Wu, X. Bu, P. Liao, L. Wang, S.-T. Zheng, R. Ma and P. Feng, *J. Am. Chem. Soc.*, 2012, **134**, 3619–3622.

119 D. Aynetdinova, M. C. Callens, H. B. Hicks, C. Y. X. Poh, B. D. A. Shennan, A. M. Boyd, Z. H. Lim, J. A. Leitch and D. J. Dixon, *Chem. Soc. Rev.*, 2021, **50**, 5517–5563.

120 Y. Chen, *Chem. – Eur. J.*, 2019, **25**, 3405–3439.

121 B. Peters, S. Santner, C. Donsbach, P. Vöpel, B. Smarsly and S. Dehnen, *Chem. Sci.*, 2019, **10**, 5211–5217.

122 B. Peters, G. Stuhrmann, F. Mack, F. Weigend and S. Dehnen, *Angew. Chem., Int. Ed.*, 2021, **60**, 17622–17628.

123 G. Stuhrmann, J. Schneider, K. Schmidt and S. Dehnen, *Chem. Commun.*, 2023, **59**, 13171–13174.

124 M. Tallu, B. Peters, A. Friedrich and S. Dehnen, *Inorg. Chem.*, 2023, **62**, 13943–13952.

125 N.-N. Shen, B. Hu, C.-C. Cheng, G.-D. Zou, Q.-Q. Hu, C.-F. Du, J.-R. Li and X.-Y. Huang, *Cryst. Growth Des.*, 2018, **18**, 962–968.

126 Y. Wang, Q. Hu, J. Jin, J. Li, J. Li and X. Huang, *Dalton Trans.*, 2020, **49**, 5020–5023.

127 Y. Wang, Z. Zhu, Z. Sun, Q. Hu, J. Li, J. Jiang and X. Huang, *Chem. – Eur. J.*, 2020, **26**, 1624–1632.

128 W.-W. Xiong, J.-R. Li, B. Hu, B. Tan, R.-F. Li and X.-Y. Huang, *Chem. Sci.*, 2012, **3**, 1200.

129 Q. Zhang, I. Chung, J. I. Jang, J. B. Ketterson and M. G. Kanatzidis, *J. Am. Chem. Soc.*, 2009, **131**, 9896–9897.

130 E. Ahmed, J. Breternitz, M. F. Groh, A. Isaeva and M. Ruck, *Eur. J. Inorg. Chem.*, 2014, 3037–3042.

131 K. Biswas, Q. Zhang, I. Chung, J.-H. Song, J. Androulakis, A. J. Freeman and M. G. Kanatzidis, *J. Am. Chem. Soc.*, 2010, **132**, 14760–14762.

132 K. Biswas, I. Chung, J.-H. Song, C. D. Malliakas, A. J. Freeman and M. G. Kanatzidis, *Inorg. Chem.*, 2013, **52**, 5657–5659.